Hindawi Publishing Corporation
Shock and Vibration
Volume 2016, Article ID 6060959, 9 pages
http://dx.doi.org/10.1155/2016/6060959

Research Article

Dynamical Model for an Interharmonic Property of a Piezoelectric Bimorph Cantilever Beam with Self-Sensing Function

Ting Zhang, Ying Pan, and Lijie Cao

College of Mechanical Engineering, Shanghai University of Engineering Science, Shanghai 201620, China

Correspondence should be addressed to Ting Zhang; ztwcl@sjtu.edu.cn

Received 3 May 2016; Revised 30 July 2016; Accepted 2 August 2016

Academic Editor: Mickaël Lallart

A piezoelectric bimorph cantilevered beam is analyzed dynamically by a longitudinal and transverse coupling theory. When a sinusoidal voltage is applied on the actuating layer of the bimorph, the output voltage of the sensing layer appears as interharmonic component signal. The interharmonic frequency is noninteger harmonic frequency of the applied voltage. A dynamic model is proposed to describe the interharmonic property of the piezoelectric bimorph beam. Through some simulations and experiments, the theoretical model is verified effectively to express the nonlinear characteristic. Furthermore, when the piezoelectric bimorph resonance happens, some interharmonic response at low frequency will modulate with the resonance response.

1. Introduction

Piezoelectric materials have been widely applied to many practical areas. The bimorph, which consisted of two pieces of piezoelectric patches bonded symmetrically on the top and bottom of a copper electrode beam, has been used as electroacoustic transducer, energy harvester, micropump driver, and microrobot for its sensitive response characteristics. For example, a bimorph impedance transducer was utilized as a simultaneous actuator and sensor for mechanical impedance measurement [1], an electromechanical piezoelectric bimorph beam with a tip mass as a power harvester under two input base transverse and longitudinal excitations extracts energy from the vibration system via piezoelectric transduction [2], and a circular piezoelectric bimorph for a micropump driver was optimized by a finite-element method [3]. However, before the piezoelectric bimorph can be used in these fields, it is necessary to study its actuating and sensing properties.

A significant number of works have thus focused on modeling the electromechanical coupling characteristics of the piezoelectric bimorph. By a finite element method the static and dynamic analysis of a piezoelectric bimorph was implemented [4], using a spectral finite element method for bimorph piezoelectric beam energy harvesters that was developed based on the Timoshenko beam theory and the Euler-Bernoulli beam theory [5], and a finite element model was developed and used to evaluate the accuracy of the analytic model for a bimorph cantilever undergoing asymmetric sensing and actuation [6], and a finite element method for a piezoelectric bimorph was used to account for the changes in physical properties of the membrane strip at the location of the piezoelectric bimorph [7]. Except for the finite element model, other methods were adopted to represent the piezoelectric bimorph mathematically; for instance, the mechanical equivalent spring mass-damper model and the electric equivalent circuit model for a piezoelectric cantilever bimorph energy harvester were compared [8], a distributed parameter piezoelectric bimorph cantilever energy harvester was modeled by an Euler-Bernoulli theory combined with the modal expansion theorem [9], a closed-form analytical solution was presented for a piezoelectric unimorph cantilever under base excitation based on the Euler-Bernoulli beam assumptions with Rayleigh-Ritz discretization [10], and an efficient spectral element with electric potential degrees of freedom was proposed to investigate

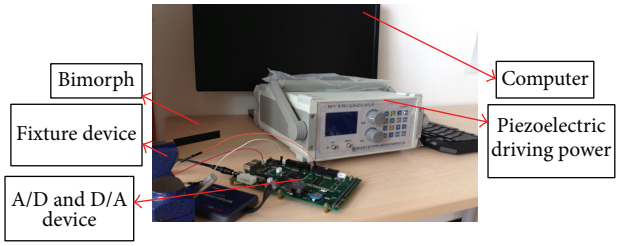

Figure 1: A vibration measure system for a piezoelectric bimorph.

the static electromechanical responses of a piezoelectric bimorph for its actuator and sensor functions [11]. However, the piezoelectric bimorph has inherent nonlinear property; macrofiber composite-based bimorph actuators inherited the nonlinear properties of hysteresis and creep of piezoelectric materials and were modeled with a hybrid model including a generalized Maxwell slip operator and a creep operator [12] and a nonlinear mathematical model for the spacecraft coupled by the hub-bimorph mechanism was developed [13].

Vibratory energy harvesters (VEHs) have been developed to exploit the sensing ability of smart materials by the electromechanical mechanisms under external vibrations. Some designed miniaturized VEHs were capable of harnessing energy efficiently from low frequency excitations. Additionally, purposeful introduction of nonlinearities into the dynamics has been investigated to enhance the broadband transduction [14]. Moreover, for a piezoelectric vibration energy harvester at suitable mechanical excitation, a nonlinear frequency-up conversion mechanism could widen the equivalent bandwidth of the piezoelectric energy converter [15].

This paper investigates a different phenomenon, namely, the interharmonic [16, 17] resonance property of a piezoelectric bimorph for the purpose of energy harvesting under low frequency excitations. Figure 1 shows a vibration response measure system for a piezoelectric bimorph, whose end is fixed with the fixture device. The piezoelectric actuating layer is applied with a sinusoidal voltage from the driving device controlled by the D/A circuit, while the piezoelectric sensing layer outputs harmonic voltage due to the stress from the actuated bending deformation. The output harmonic voltage is saved by the computer through the A/D circuit. Figure 2 gives the harmonic voltage signal and frequency response by the Fast Fourier Transform when a sinusoidal voltage at amplitude 4.5 V and frequency 1.4 Hz is applied on the actuating layer. The output voltage is shown in Figure 2(a), and it indicates a modulated wave signal which includes many frequency sinusoidal signals. Figure 2(b) displays the magnitude-frequency characteristics of the output voltage, and it is manifested that the output voltage has multiple interharmonic components, and the first four frequencies are 1.404 Hz, 2.698 Hz, 5.507 Hz, and 6.801 Hz, respectively. Therefore, it is necessary that this interharmonic property of the piezoelectric bimorph is described mathematically and accurately before it is widely used in a variety of areas.

The rest of this paper is organized as follows: In Section 2, the interharmonic property model of the piezoelectric bimorph cantilevered beam is introduced. In Section 3, the simulation and experiment results are shown, and some discussions are focused. Finally some conclusions are given in Section 4.

2. Dynamical Model for a Piezoelectric Bimorph Cantilever Beam

Figure 3 shows a piezoelectric bimorph cantilever beam. The left end of the beam is fixed and the right end is free. Moreover, the layers above and below are the piezoelectric (PZT) material and the middle layer is a copper electrode. l_b and h_b are effective length and height of the cantilever beam, respectively. Furthermore, h_e is height of the electrode and x_p is the distance from the fixture to the piezoelectric materials. The bimorph is mainly used to detect and suppress vibration signal for space structures. Therefore, the sensing property integrated with actuating function of the piezoelectric bimorph will be modeled by some dynamic analyses.

An infinitesimal element method is proposed to model the nonlinear bifurcation property for the bimorph shown in Figure 4. N, Q, and M are the axial force, the shear force, and the bending moment, respectively. Moreover, θ is the angle between the x-axis and the center axis of the bimorph. And ds is the length of the infinitesimal element. "a", "e," and "s" represent "actuating layer," "electrode layer," and "sensing layer," respectively. A set of equations is gained by force balance principle and is expressed as

$$\begin{aligned}
&\left(N+\frac{\partial N}{\partial s}ds\right)\cos\left(\theta+\frac{\partial\theta}{\partial s}ds\right)-N\cos(\theta)\\
&\quad+\left(Q+\frac{\partial Q}{\partial s}ds\right)\sin\left(\theta+\frac{\partial\theta}{\partial s}ds\right)-Q\sin(\theta)-c\dot{u}_x\\
&\quad+f_x=dm\ddot{u}_x,\\
&\left(N+\frac{\partial N}{\partial s}ds\right)\sin\left(\theta+\frac{\partial\theta}{\partial s}ds\right)-N\sin(\theta)\\
&\quad+\left(Q+\frac{\partial Q}{\partial s}ds\right)\cos\left(\theta+\frac{\partial\theta}{\partial s}ds\right)-Q\cos(\theta)-c\dot{u}_y\\
&\quad+f_y=dm\ddot{u}_y,
\end{aligned}\tag{1}$$

where u_x and u_y are displacements along the x-axis and the y-axis, respectively. $\dot{u}$ and $\ddot{u}$ are time differential variables. f is an external force. Furthermore $dm = \rho A ds$ and $ds = dx/\cos(\theta)$, and ρ is density. A is the cross-sectional area of the infinitesimal element. The relation between the shear force Q and the bending moment M is given as

$$Q=\frac{\partial M}{\partial s}=\frac{\partial M}{\partial x}\cos(\theta).\tag{2}$$

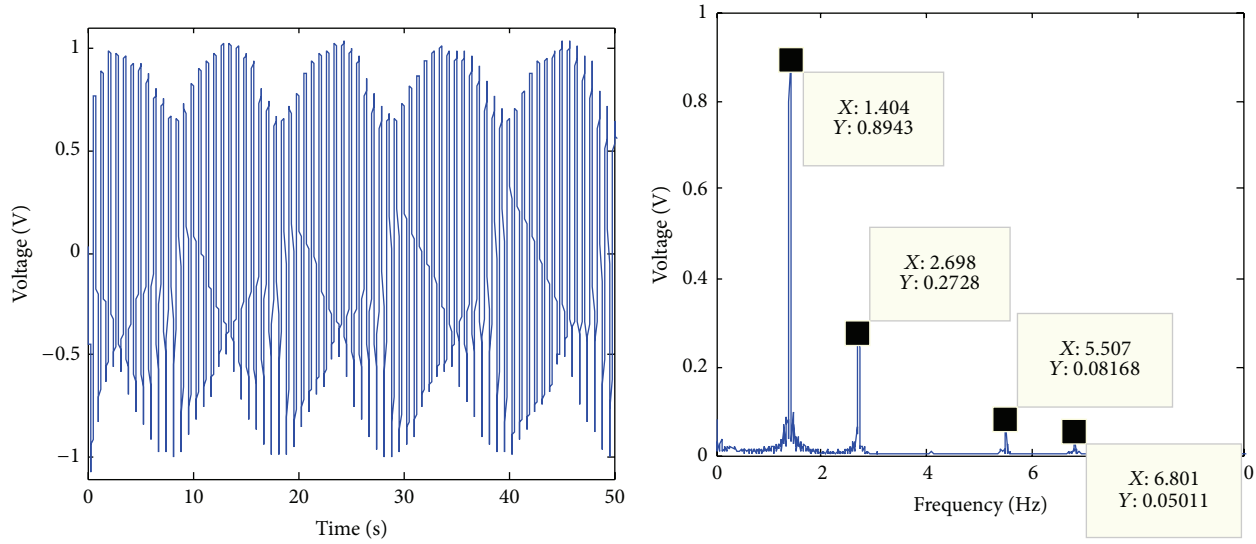

(a) Time response (b) Frequency response

Figure 2: Interharmonics response.

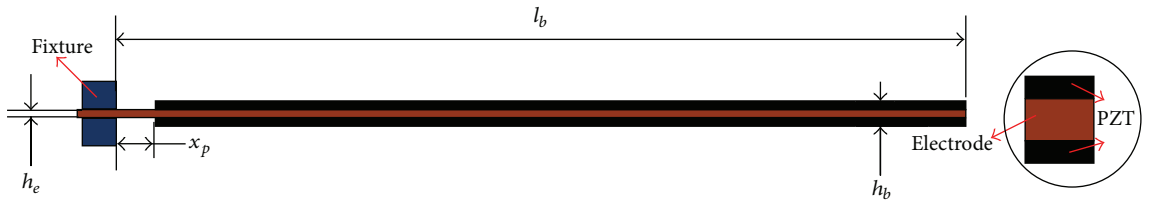

Figure 3: A piezoelectric bimorph cantilever beam.

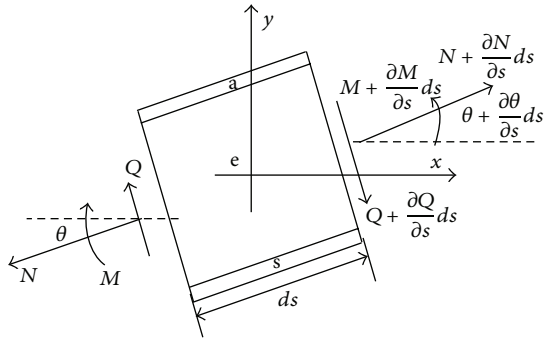

Figure 4: Infinitesimal element of the bimorph.

Therefore submitting dm, ds, and (2) into (1), and having $\theta + (\partial\theta/\partial s)ds \approx \theta$, (1) may be transformed as

$$\begin{aligned} &\frac{\partial}{\partial s}\left[N\cos(\theta) + \frac{\partial M}{\partial x}\cos(\theta)\sin(\theta)\right] + f_x \\ &\quad = \rho A\ddot{u}_x + c\dot{u}_x, \\ &\frac{\partial}{\partial s}\left[N\sin(\theta) + \frac{\partial M}{\partial x}\cos(\theta)\cos(\theta)\right] + f_y \\ &\quad = \rho A\ddot{u}_y + c\dot{u}_y. \end{aligned} \tag{3}$$

Then, because of $\tan(\theta) = \partial u_y/\partial x$, $\tan(\theta) \approx \sin(\theta) \approx \theta$ when $\theta \to 0$. Moreover, the trigonometrical functions are expanded with the Taylor series; namely, $\cos(\theta) = 1 - (1/2)(\theta)^2 + o(\theta^2)$. Therefore

$$\begin{aligned} \sin(\theta) &\approx \frac{\partial u_y}{\partial x}, \\ \cos(\theta) &\approx 1 - \frac{1}{2}\left(\frac{\partial u_y}{\partial x}\right)^2. \end{aligned} \tag{4}$$

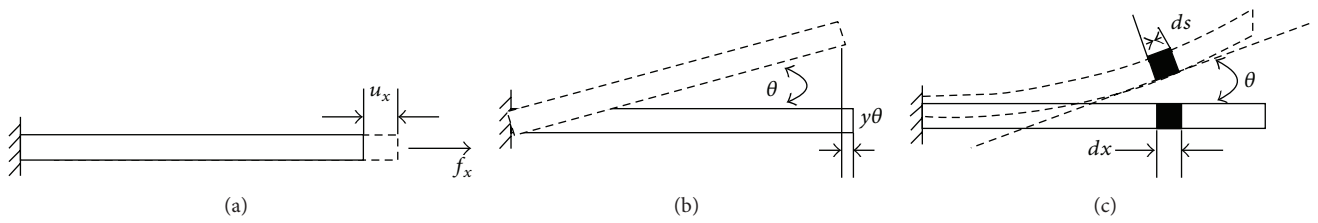

Figure 5: Longitudinal displacement.

In addition, the longitudinal displacement $u_l(x,z,t)$ consisted of three parts. The first part is the axial displacement $u_x(x,t)$ by the transversal force f_x shown in Figure 5(a), Figure 5(b) displays the second part $y\cdot\tan(\theta)\approx y\theta$ caused by the cross-sectional rotation, and Figure 5(c) shows the third part $(s-x)$ from the lateral curvature; it is given as

$$\begin{aligned} s-x &= \int_0^x ds - x = \int_0^x \frac{dx}{\cos(\theta)} - x \\ &= \int_0^x \sqrt{\left[1+\tan^2(\theta)\right]}dx - x \\ &= \int_0^x \sqrt{1+\left(\frac{\partial u_y}{\partial x}\right)^2}\,dx - x. \end{aligned} \tag{5}$$

Therefore, u_l is derived as

$$u_l = u_x + y\theta + \int_0^x \sqrt{1+\left(\frac{\partial u_y}{\partial x}\right)^2}\,dx - x. \tag{6}$$

And the corresponding stress is expressed as

$$\sigma_l = E\frac{\partial u_l}{\partial s} = E\frac{\partial u_l}{\partial x}\cos(\theta), \tag{7}$$

where $E = E_e + 2E_a$, where E_e and E_a are the Young modulus of the electrode and piezoelectric material, respectively.

Moreover, the actuating stress is generated by the applied voltage V on the piezoelectric layer and is described as

$$\begin{aligned} \varepsilon_1 &= s_{11}^E\sigma_1 + d_{31}E_3, \\ D_3 &= d_{31}\sigma_1 + \varepsilon_{33}^S E_3, \end{aligned} \tag{8}$$

where A_a is the cross-sectional area of the piezoelectric actuating layer and $E_3 = V(x,t)/h_a$, where $V(x,t)$ is Heaviside function. h_a is thickness of the piezoelectric actuating layer.

Hence, with (7) and (8), the axial force is derived as

$$\begin{aligned} N(x,t) &= \iint_A (\sigma_l + \sigma_1)\,dA \\ &= EA\left[\frac{\partial u_x}{\partial x} + \frac{1}{2}\left(\frac{\partial u_y}{\partial x}\right)^2\right]\cos(\theta) \\ &\quad + E_a d_{31} A_a \frac{V}{h_a}. \end{aligned} \tag{9}$$

And the bending moment is gained as

$$\begin{aligned} M(x,t) &= \iint_A (\sigma_l + \sigma_1)\, y\,dA \\ &= EI\frac{\partial\theta}{\partial x}\cos(\theta) + E_a d_{31} A_a \frac{V}{2h_a}\left(h_e + h_a\right), \end{aligned} \tag{10}$$

where

$$\frac{\partial\theta}{\partial x} = \left[\cos(\theta)\right]^2 \frac{\partial^2 u_y}{\partial x^2}. \tag{11}$$

And

$$N_V(x,t) = EA\frac{\partial u_x(x,t)}{\partial x} = E_a d_{31} A_a \frac{V(x,t)}{h_a}. \tag{12}$$

Assuming $f_x = 0$ and $f_y = 0$, substitute (9) and (10) into (3), and then

$$\begin{aligned} &\rho A\frac{\partial^2 u_y}{\partial t^2} + c\frac{\partial u_y}{\partial t} + EI\frac{\partial^4 u_y}{\partial x^4} - 3EI\left(\frac{\partial^2 u_y}{\partial x^2}\right)^3 \\ &\quad \approx 2v_N V\frac{\partial^2 u_y}{\partial x^2} + v_M\frac{\partial^2 V}{\partial x^2} - v_M V\left(\frac{\partial^2 u_y}{\partial x^2}\right)^2, \end{aligned} \tag{13}$$

where

$$\begin{aligned} v_N &= \frac{E_a d_{31} A_a}{h_a}, \\ v_M &= E_a d_{31} A_a \frac{\left(h_e + h_a\right)}{2h_a}, \\ u_y &= \phi(x)\,q(t), \end{aligned} \tag{14}$$

where

$$\begin{aligned} &\phi(x) \\ &\quad = \cos\frac{ax}{l} - \operatorname{ch}\frac{ax}{l} \\ &\qquad + \frac{\sin(a) - \operatorname{sh}(a)}{\cos(a) + \operatorname{ch}(a)}\left(\sin\frac{ax}{l} - \operatorname{sh}\frac{ax}{l}\right), \\ &1 + \cos(a)\operatorname{ch}(a) = 0, \\ &a = 1.875, \\ &M\ddot{q} + C\dot{q} + Kq - \alpha q^3 = \left(\kappa + \beta q + \gamma q^2\right)V_i, \end{aligned} \tag{15}$$

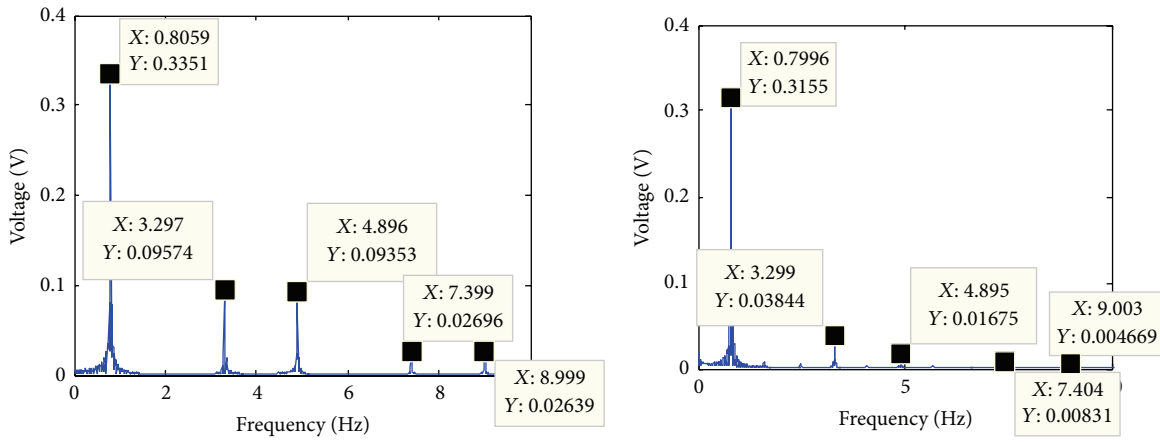

(a) Simulation (b) Experiment

Figure 6: Frequency response at 0.8 Hz.

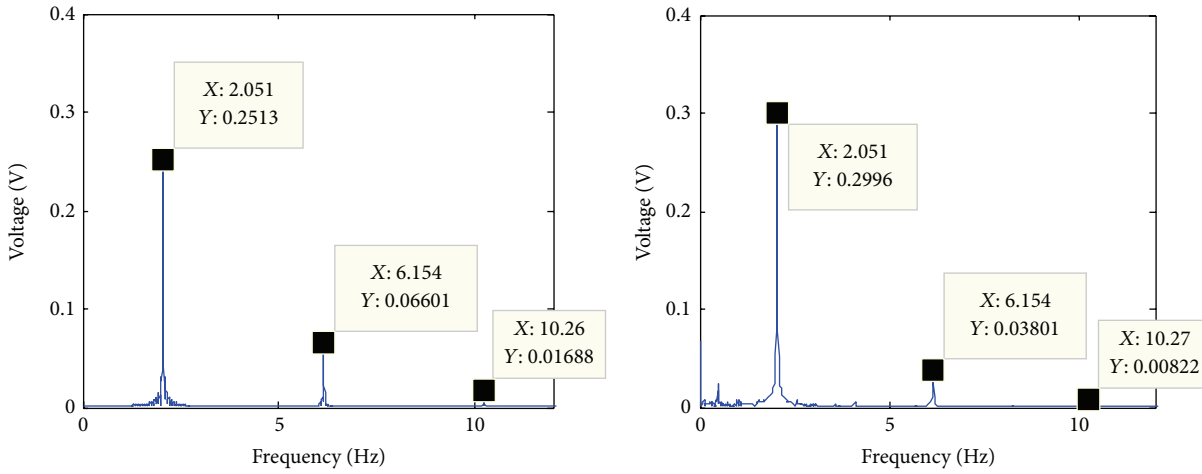

(a) Simulation (b) Experiment

Figure 7: Frequency response at 2.05 Hz.

where

$$
\begin{aligned}
M &= \int_0^{l_b} \rho A \varphi(x)\, dx, \\
C &= \int_0^{l_b} c \varphi(x)\, dx, \\
K &= \int_0^{l_b} EI \frac{\partial^4 \varphi(x)}{\partial x^4} dx, \\
\alpha &= \int_0^{l_b} 3EI \frac{\partial^2 \varphi(x)}{\partial x} dx, \\
\kappa &= v_M, \\
\beta &= 2 \int_0^{l_b} v_N \frac{\partial \varphi^2(x)}{\partial x^2} dx, \\
\gamma &= -\int_0^{l_b} v_M \left[\frac{\partial^2 \varphi(x)}{\partial x} \right]^2 dx, \\
V_i &= V\left(x_p, t\right).
\end{aligned}
\tag{16}
$$

The output voltage V_o of the sensing layer is given in [14]. Therefore, the describing set of equations of the interharmonic property for piezoelectric bimorph is expressed as

$$
\begin{aligned}
M\ddot{q} + C\dot{q} + Kq - \alpha q^3 + \mu V_o &= \left(\kappa + \beta q + \gamma q^2\right) V_i, \\
-\mu \dot{q} + c_s \dot{V}_o + \frac{V_o}{R} &= 0,
\end{aligned}
\tag{17}
$$

where μ is the electromechanical coupling, c_s is the effective capacitance of the piezoelectric sensing layers, and R is the electric load and is equal to $R_l(1 - r \sin 2\pi f_R)$, where R_l is a load's resistance, r is a corresponding coefficient, and f_R is the load's frequency.

3. Results and Discussions

Based on the constructed model (17), the simulation and experiment results are shown in Figures 6–9 with the Fast Fourier Transform Algorithm. Figure 6 gives the frequency response when the applied voltage frequency of the actuating piezoelectric layer is 0.8 Hz. The frequencies of simulation

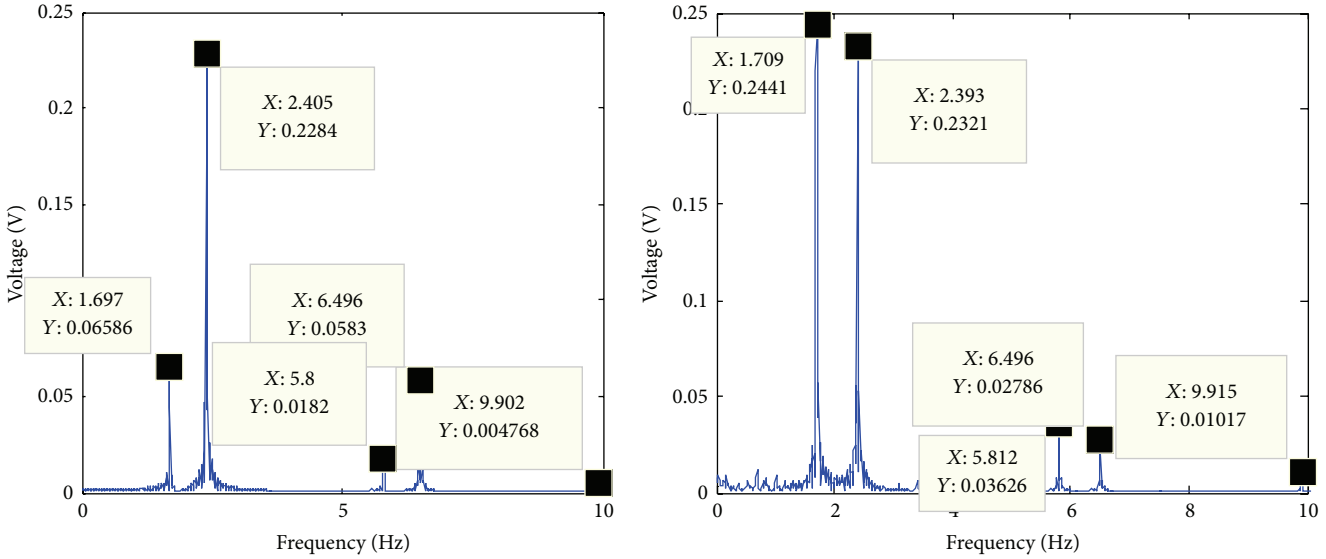

(a) Simulation (b) Experiment

Figure 8: Frequency response at 2.4 Hz.

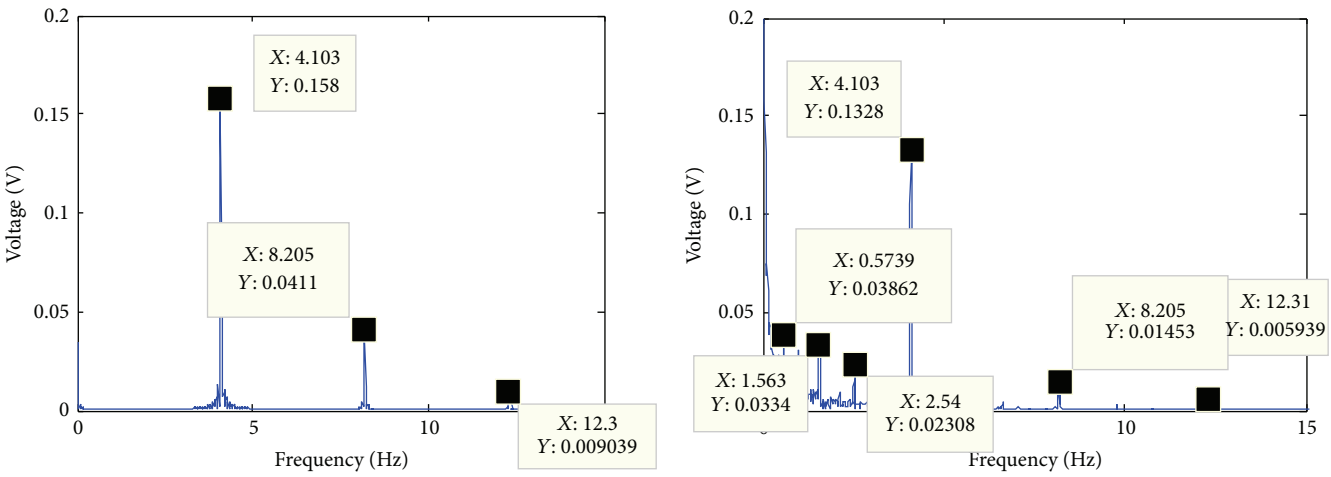

(a) Simulation (b) Experiment

Figure 9: Frequency response at 4.1 Hz.

response in Figure 6(a) are 0.8059 Hz, 3.297 Hz, 4.896 Hz, 7.399 Hz, and 8.999 Hz while the response frequencies of experiment in Figure 6(b) are 0.7996 Hz, 3.299 Hz, 4.895 Hz, 7.404 Hz, and 9.003 Hz. Moreover, Figure 7 shows the frequency response at the input voltage frequency 2.05 Hz. The simulation output frequencies in Figure 7(a) are 2.051 Hz, 6.154 Hz, and 10.26 Hz and the experiment output frequencies in Figure 7(b) are 2.051 Hz, 6.154 Hz, and 10.27 Hz. Furthermore, Figure 8 displays the frequency response when the actuating voltage frequency is 2.4 Hz. The response frequencies with simulation in Figure 8(a) are 1.679 Hz, 2.405 Hz, 5.8 Hz, 6.496 Hz, and 9.902 Hz while the output response frequencies with experiment are 1.709 Hz, 2.393 Hz, 5.812 Hz, 6.496 Hz, and 9.915 Hz in Figure 8(b). Finally, when the applied voltage frequency of the actuating piezoelectric layer is 4.1 Hz, the output response voltage frequencies are given in Figure 9. The simulation output voltage frequencies in Figure 9(a) are 4.103 Hz, 8.205 Hz, and 12.3 Hz and the experiment output voltage frequencies are 0.5739 Hz, 0.989 Hz 1.563 Hz, 2.54 Hz, 4.103 Hz, 8.205 Hz, and 12.31 Hz in Figure 9(b).

Therefore, from above discussion on comparison between the simulation and experiment results, the law of the output voltage frequency from the sensing piezoelectric layer is summarized from the four set results at different input voltage frequencies and is shown in Table 1. The output voltage frequencies are $f_i, f_R \pm f_i, 2f_R \pm f_i, 3f_R \pm f_i, \ldots$, and $f_R = 4.10$ Hz. If f_R is not equal to f_i, the interharmonics will appear. When

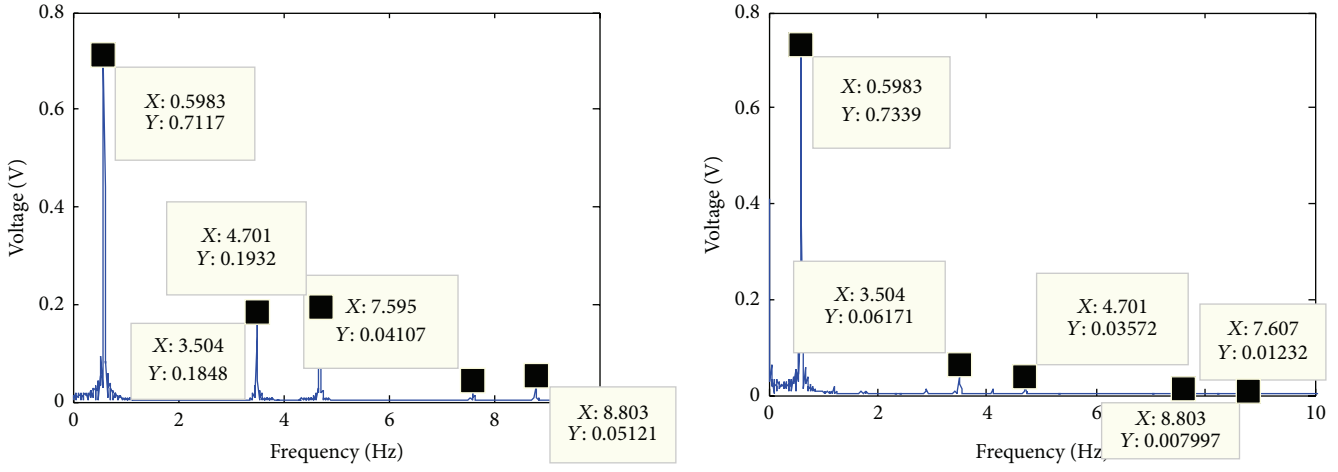

(a) Simulation (b) Experiment

Figure 10: Frequency response at 0.6 Hz.

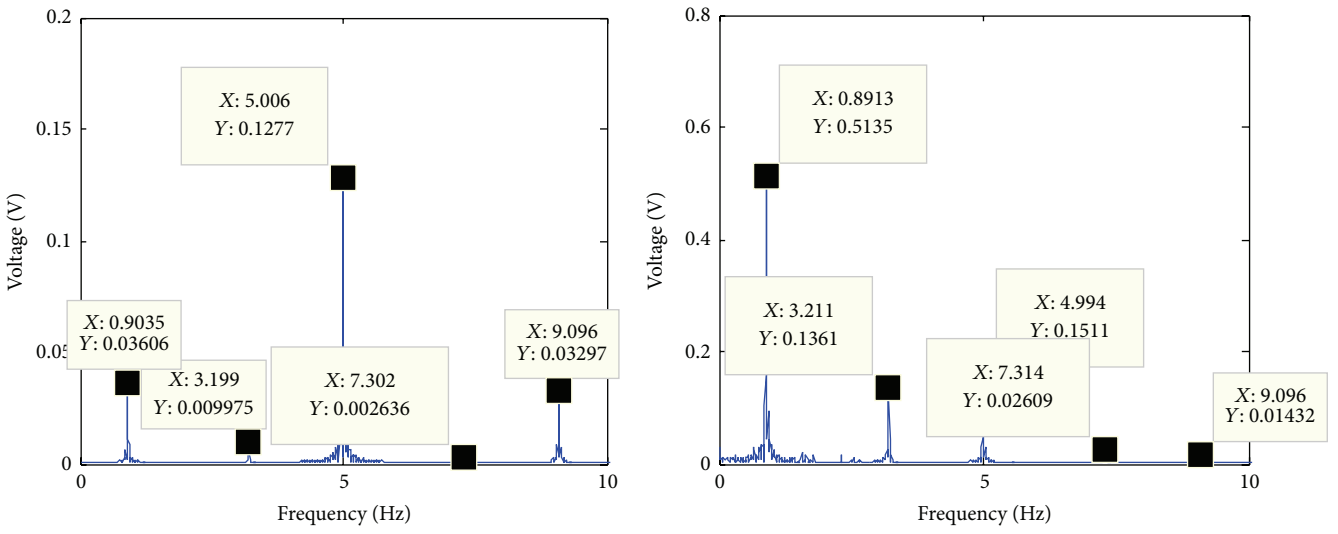

(a) Simulation (b) Experiment

Figure 11: Frequency response at 5 Hz.

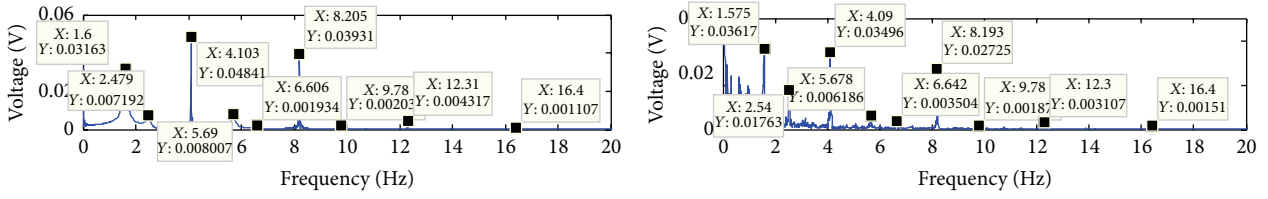

(a) Simulation (b) Experiment

Figure 12: Frequency response at 8.2 Hz.

f_R is equal to f_i, the resonance phenomenon will happen. Then, that output voltage frequency f_o may be deduced at input frequencies 0.6 Hz, 5 Hz, and 8.2 Hz. Shown in Figures 10–12, the frequency responses by simulations are compared with experiments. And the compared frequency results are given in Tables 2 and 3. From Figure 10, when the input voltage is applied with a sinusoidal signal at amplitude 4.5 V and frequency 0.6 Hz, the frequencies of output response are 0.5983 Hz, 3.504 Hz, 4.701 Hz, 7.595 Hz, and 8.803 Hz by simulations and 0.5983 Hz, 3.504 Hz, 4.701 Hz, 7.607 Hz,

Table 1: Output frequency of voltage response.

f_i (Hz)	f_o (Hz)							
	f_{sup1}	f_{sup2}	f_{sup3}	f_{sup4}	f_1	f_{sub1}	f_{sub2}	f_{sub3}
0.80					0.80	3.30	4.90	7.40
2.05					2.05	6.15	10.26	
2.40				1.70	2.40	5.80	6.50	9.90
4.10	0.57	0.99	1.56	2.54	4.10	8.20	12.30	

Table 2: Simulation output frequency.

f_i (Hz)	f_o (Hz)								
	f_{sup1}	f_{sup2}	f_{sup3}	f_{sup4}	f_1	f_{sub1}	f_{sub2}	f_{sub3}	f_{sub4}
0.6					0.598	3.504	4.701	7.595	8.803
5.0				0.9035	3.199	5.006	7.302	9.096	
8.2	1.600	2.479	4.103	5.690	6.606	8.205	9.780	12.310	16.40

and 8.803 Hz by experiments, respectively. Similarly, From Figure 11, when the input voltage is applied with a sinusoidal signal at amplitude 4.5 V and frequency 5 Hz, the frequencies of output response are 0.9035 Hz, 3.199 Hz, 5.006 Hz, 7.302 Hz, and 9.096 Hz by simulations and 0.8913 Hz, 3.211 Hz, 4.994 Hz, 7.314 Hz, and 9.096 Hz by experiments, respectively. And from Figure 12, when the input voltage is applied with a sinusoidal signal at amplitude 4.5 V and frequency 8.2 Hz, the frequencies of output response are 1.6 Hz, 2.479 Hz, 4.103 Hz, 5.69 Hz, 6.606 Hz, 8.205 Hz, 9.78 Hz, 12.31 Hz, and 16.4 Hz by simulations and 1.575 Hz, 2.54 Hz, 4.09 Hz, 5.678 Hz, 6.642 Hz, 8.193 Hz, 9.78 Hz, 12.3 Hz, and 16.4 Hz by experiments, respectively. The corresponding output frequency results are displayed in Table 2 with simulations and Table 3 with experiments, respectively.

Therefore, the interharmonics property of the piezoelectric bimorph is reflected not only in the smaller frequency but also in the higher frequency of the output response than that of input voltage. Moreover the theoretical model of the piezoelectric bimorph is verified effectively by simulations and experiments. Furthermore, the output simulation frequencies are almost the same as the output experimental frequencies. Especially when the input voltage is at frequency $4.1 \times n$ Hz ($n = 1, 2, 3, \ldots$), the output response voltage has resonance and lower frequency interharmonics.

4. Conclusions

In the paper, a theoretical model is proposed for a piezoelectric bimorph to describe the interharmonic property. And the dynamic model is constructed by the longitudinal and transverse coupling theory for the piezoelectric bimorph cantilevered beam. Moreover, with the simulation and experiment results, the theoretical model is validated to express the nonlinear characteristic. Furthermore, in future work, the theoretical model will be used to design a displacement compensating controller for the piezoelectric bimorph cantilevered beam.

Table 3: Experiment output frequency.

f_i (Hz)	f_o (Hz)								
	f_{sup1}	f_{sup2}	f_{sup3}	f_{sup4}	f_1	f_{sub1}	f_{sub2}	f_{sub3}	f_{sub4}
0.6					0.598	3.504	4.701	7.607	8.803
5.0				0.891	3.211	4.994	7.314	9.096	
8.2	1.575	2.540	4.090	5.678	6.642	8.193	9.780	12.300	16.400

Competing Interests

The authors declare that there is no conflict of interests regarding the publication of this paper.

Acknowledgments

This work was supported by the Scientific Research Startup Foundation of Shanghai University of Engineering Science and the Shanghai Science and Technology commission local colleges' capacity building project: 14110501200.

References

[1] X. Hou, "Modeling and characterization of a bimorph impedance transducer," *Journal of Sound and Vibration*, vol. 324, no. 3–5, pp. 608–621, 2009.

[2] M. F. Lumentut and I. M. Howard, "Analytical and experimental comparisons of electromechanical vibration response of a piezoelectric bimorph beam for power harvesting," *Mechanical Systems and Signal Processing*, vol. 36, no. 1, pp. 66–86, 2013.

[3] C. J. Morris and F. K. Forster, "Optimization of a circular piezoelectric bimorph for a micropump driver," *Journal of Micromechanics and Microengineering*, vol. 10, no. 3, pp. 459–465, 2000.

[4] S. Y. Wang, "A finite element model for the static and dynamic analysis of a piezoelectric bimorph," *International Journal of Solids and Structures*, vol. 41, no. 15, pp. 4075–4096, 2004.

[5] G. Wang, "Analysis of bimorph piezoelectric beam energy harvesters using Timoshenko and Euler-Bernoulli beam theory," *Journal of Intelligent Material Systems and Structures*, vol. 24, no. 2, pp. 226–239, 2013.

[6] P. J. Costa Branco and J. A. Dente, "On the electromechanics of a piezoelectric transducer using a bimorph cantilever undergoing asymmetric sensing and actuation," *Smart Materials and Structures*, vol. 13, no. 4, pp. 631–642, 2004.

[7] J. M. Renno and D. J. Inman, "An experimentally verified model of a membrane mirror strip actuated using piezoelectric bimorph," *Journal of Vibration and Acoustics*, vol. 129, no. 5, pp. 631–640, 2007.

[8] L. Zhang, K. A. Williams, and Z. Xie, "Development and validation of an enhanced coupled-field model for PZT cantilever bimorph energy harvester," *Mathematical Problems in Engineering*, vol. 2013, Article ID 980161, 10 pages, 2013.

[9] S. Rafique and P. Bonello, "Experimental validation of a distributed parameter piezoelectric bimorph cantilever energy harvester," *Smart Materials and Structures*, vol. 19, no. 9, article 094008, 2010.

[10] A. Erturk and D. J. Inman, "An experimentally validated bimorph cantilever model for piezoelectric energy harvesting from base excitations," *Smart Materials and Structures*, vol. 18, no. 2, Article ID 025009, 19 pages, 2009.

[11] X. J. Dong, Z. K. Peng, H. X. Hua, and G. Meng, "Modeling of the through-the-thickness electric potentials of a piezoelectric bimorph using the spectral element method," *Sensors*, vol. 14, no. 2, pp. 3477–3492, 2014.

[12] C. Zhang, J. Qiu, Y. Chen, and H. Ji, "Modeling hysteresis and creep behavior of macrofiber composite-based piezoelectric bimorph actuator," *Journal of Intelligent Material Systems and Structures*, vol. 24, no. 3, pp. 369–377, 2013.

[13] Y.-L. Kuo, "Attitude control of miniature spacecraft under the gravitational effect using a hub-bimorph mechanism," *Journal of Vibration and Control*, vol. 19, no. 12, pp. 1822–1832, 2013.

[14] R. Masana and M. F. Daqaq, "Energy harvesting in the super-harmonic frequency region of a twin-well oscillator," *Journal of Applied Physics*, vol. 111, no. 4, Article ID 044501, 2012.

[15] M. Ferrari, M. Baù, F. Cerini, and V. Ferrari, "Impact-enhanced multi-beam piezoelectric converter for energy harvesting in autonomous sensors," *Procedia Engineering*, vol. 47, pp. 418–421, 2012.

[16] S. Djurovic, D. S. Vilchis-Rodriguez, and A. C. Smith, "Supply induced interharmonic effects in wound rotor and doubly-fed induction generators," *IEEE Transactions on Energy Conversion*, vol. 30, no. 4, pp. 1397–1408, 2015.

[17] K. S. Smith and L. Ran, "Torsional resonance risk management in islanded industrial power systems supplying large VFDs," *IEEE Transactions on Industry Applications*, vol. 44, no. 6, pp. 1841–1850, 2008.